Journal of Power Sources 195 (2010) 1001–1006

Contents lists available at ScienceDirect

Journal of Power Sources

journal homepage: www.elsevier.com/locate/jpowsour

Synthesis of PdNi catalysts for the oxidation of ethanol in alkaline direct ethanol fuel cells

S.Y. Shen, T.S. Zhao*, J.B. Xu, Y.S. Li

Department of Mechanical Engineering, The Hong Kong University of Science and Technology, Clear Water Bay, Kowloon, Hong Kong SAR, China

ARTICLE INFO

Article history:
Received 1 June 2009
Received in revised form 6 August 2009
Accepted 20 August 2009
Available online 2 September 2009

Keywords:
Fuel cell
Alkaline direct ethanol fuel cell
Ethanol oxidation reaction
Palladium catalyst
Palladium–nickel catalyst

ABSTRACT

Carbon-supported PdNi catalysts for the ethanol oxidation reaction in alkaline direct ethanol fuel cells are successfully synthesized by the simultaneous reduction method using $NaBH_4$ as reductant. X-ray diffraction characterization confirms the formation of the face-centered cubic crystalline Pd and $Ni(OH)_2$ on the carbon powder for the PdNi/C catalysts. Transmission electron microscopy images show that the metal particles are well-dispersed on the carbon powder, while energy-dispersive X-ray spectrometer results indicate the uniform distribution of Ni around Pd. X-ray photoelectron spectroscopy analyses reveal the chemical states of Ni, including metallic Ni, NiO, $Ni(OH)_2$ and NiOOH. Cyclic voltammetry and chronopotentiometry tests demonstrate that the Pd_2Ni_3/C catalyst exhibits higher activity and stability for the ethanol oxidation reaction in an alkaline medium than does the Pd/C catalyst. Fuel cell performance tests show that the application of Pd_2Ni_3/C as the anode catalyst of an alkaline direct ethanol fuel cell with an anion-exchange membrane can yield a maximum power density of 90 mW cm^{-2} at 60 °C.

1. Introduction

Both direct methanol fuel cells (DMFCs) and direct ethanol fuel cells (DEFCs) have been projected to be strong candidates to compete with advanced batteries for powering mobile and portable electronic devices owing to their uniquely high specific energy. Since methanol is the simplest alcohol and its electrochemical reaction kinetics is faster than those of other alcohol fuels, DMFCs have been extensively studied over the past decade. The toxicity of methanol, however, limits the wide spread use by consumers. By contrast, ethanol is a more attractive fuel for low-temperature fuel cells because it is much less toxic than methanol. Moreover, ethanol can be produced in large quantities from agricultural products or biomass. For these reasons, DEFCs have recently been receiving increased attention [1,2].

A significant challenge in the development of DEFC technology is the need for highly active catalysts for the ethanol oxidation reaction (EOR) that takes place at the negative electrode (anode). The complete oxidation per ethanol molecule to CO_2 involves the release of 12 electrons and the cleavage of the C–C bond, which is between two atoms with little electron affinity or ionization energy, thus making it difficult to employ low temperatures. Previous studies have shown that the major products of the EOR in acidic media are acetaldehyde and acetic acid, which, involve the release of only two and four electrons, respectively [3–5]. Pt is the best-known material for the dissociative adsorption of small organic molecules at low temperatures. Compared with Pt, PtSn-based catalysts (both binary and ternary) show a superior catalytic activity toward the EOR in acidic media. This can be attributed to the bifunctional mechanism and an electronic effect, similar to that in the methanol oxidation reaction (MOR) on the PtRu catalyst [6,7].

Recently, with the emergence of alkaline membranes that conduct hydroxide ions (OH^-), alkaline direct alcohol fuel cells (DAFCs) have attracted interest. The most significant advantage associated with the change in the electrolyte membrane from acid to base is that the reaction kinetics of both the alcohol anodic oxidation and the oxygen cathodic reduction in alkaline media become faster than in acidic media, thus making it possible to use non-noble metal catalysts and to reduce the catalyst loading [8–10]. In this regard, Pd and Pd-based catalysts are emerging as an alternative to Pt-based catalysts for the alcohol oxidation reaction, and especially for the EOR in alkaline media [11–14]. Since Pd is more abundant in nature than Pt, the catalyst cost can be substantially reduced. Shen and co-workers [15,16] prepared a series of metal oxide (CeO_2, NiO, Co_3O_4, and Mn_3O_4) promoted Pd catalysts by means of intermittent microwave heating (IMH) method. Compared with Pt, these catalysts exhibited higher activity and stability toward the EOR in alkaline media; NiO promoted Pd catalysts were found to give the best performance. The improvement was attributed to the fact that OH_{ads} could easily form on the introduced metal oxides, which functions in the same manner as Ru in a PtRu catalyst, thus enhancing the anti-poisoning ability. With the two-step

* Corresponding author. Tel.: +852 2358 8647.
E-mail address: metzhao@ust.hk (T.S. Zhao).

0378-7753/$ – see front matter © 2009 Elsevier B.V. All rights reserved.
doi:10.1016/j.jpowsour.2009.08.079

preparation method, however, it is difficult to control the size and morphology of the metal oxides, which will result in poor contacts between Pd and carbon powder and thus sacrifice some of the active sites of the synthesized catalyst [17]. On the other hand, the inclusion of Ni in Pt, PtRu or PtSn using the simultaneous method can greatly enhance the catalytic activity and stability toward the MOR and EOR in acidic media because of the combined effect of the oxygen donation from Ni oxide/hydroxide and the change of electronic structure of Pt by electron transfer from Ni to Pt [18–21].

In this work, carbon-supported PdNi nanoparticles are synthesized by the simultaneous method using $NaBH_4$ as a reductant. For comparison, carbon-supported Pd nanoparticles are also prepared by the same method in the absence of the Ni precursor. The obtained Pd/C and PdNi/C are characterized with X-ray diffraction (XRD), transmission electron microscopy (TEM), energy-dispersive X-ray spectrometry (EDS), inductively coupled plasma atomic emission spectroscopy (ICP-AES) and X-ray photoelectron spectroscopy (XPS). The catalytic activity and stability of the Pd/C and PdNi/C catalysts are investigated by cyclic voltammetry (CV) and chronopotentiometry (CP) methods through the EOR in alkaline media. In addition to these characterizations, the performance of the Pd/C and Pd_2Ni_3/C catalysts is also tested in an in-house fabricated alkaline DEFC. It is worth mentioning that few past studies tested the catalysts for the EOR in alkaline DEFCs, except for the work by Bianchini et al. [13], who examined the anode Pd/C catalyst in an alkaline DAFC fed with methanol, ethanol or glycerol.

2. Experimental

2.1. Preparation of the Pd/C and PdNi/C catalysts

Carbon-supported Pd and PdNi nanoparticles with different Pd/Ni atomic ratios were synthesized by the simultaneous reduction method using $NaBH_4$ as a reductant. All the chemicals were of analytical grade. Palladium chloride ($PdCl_2$) (from Aldrich), nickel chloride-6-hydrate ($NiCl_2{\cdot}6H_2O$), potassium hydroxide (KOH), sodium borohydride ($NaBH_4$), hydrochloric acid (HCl), and ethanol (CH_3CH_2OH) (all from Merck KGaA) were used as-received. Vulcan XC-72 carbon (particle size 20–40 nm) was purchased from E-TEK, while 5 wt.% polytetrafluoroethylene (PTFE) emulsion was received from Dupont. The metal precursors of $PdCl_2$ and $NiCl_2{\cdot}6H_2O$ with different atomic ratios were first dissolved completely in deionized (DI) water. Carbon powders were then suspended in the resulting solution under vigorous stirring. After a homogeneous suspension was formed, 2 wt.% $NaBH_4$ was added to the mixture under steady stirring. The resulted precipitate was collected by filtration, washed several times with DI water and dried at 70 °C in an oven. For comparison, both the Pd/C and PdNi/C catalysts were guaranteed with a 20 wt.% Pd loading.

2.2. Material structure characterizations

The XRD patterns of the Pd/C and PdNi/C catalysts were obtained with a Philips powder diffraction system (model PW 1830) using a Cu Kα source operating at 40 keV at a scan rate of $0.025^\circ\ s^{-1}$. The TEM images were obtained with a high-resolution JEOL 2010F TEM system that operated with a LaB6 filament at 200 kV. The Pd:Ni atomic ratio was analyzed by EDS, which was integrated with the TEM instrument. In addition, ICP-AES analysis was conducted on a Perkin Elmer ICP-AES Spectrometer Optima 3000 XL to confirm the bulk composition of the PdNi/C catalysts. The XPS characterization was carried out with a Physical Electronics PHI 5600 multi-technique system using Al monochromatic X-rays at a power of 350 W. The survey and regional spectra were obtained by passing an energy of 187.85 and 23.5 eV, respectively.

2.3. Electrochemical characterizations

Both CV and CP were carried out with a potentiostat (EG&G Princeton, model 273A) in a conventional three-electrode cell, in which a glass carbon electrode (GCE) with an area of $0.1256\ cm^2$ was used as the underlying support for the working electrode, a platinum foil as the counter electrode, and Hg/HgO/KOH ($1.0\ mol\ L^{-1}$) (MMO, 0.098 V vs. SHE) as the reference electrode, which was connected to the cell through a Luggin capillary. The GCE was modified by depositing a catalyst layer on it and served as the working electrode. The catalyst ink was prepared by ultrasonically dispersing 10 mg of 20 wt.% Pd/C or PdNi/C in 1.9 mL of ethanol, to which 0.1 mL of 5 wt.% PTFE emulsion was added. After 30 min, a homogeneous solution was obtained and 24 μL of the ink was pipetted on top of the GCE and dried in air to yield a Pd loading of $191\ \mu g\ cm^{-2}$. Solutions were prepared from analytical grade reagents and DI water. All the CV and CP experiments were performed at room temperature and in a 1.0 M KOH solution containing 1.0 M ethanol, which was deaerated by bubbling nitrogen (99.9%) for 30 min in advance. The CV tests were performed between the potential range of −0.926 to 0.274 V at a scan rate of $50\ mV\ s^{-1}$ and the CP tests were conducted at the current density of $20\ mA\ cm^{-2}$ for 12 h. The potentials in this work all refer to the MMO, and the current densities were calculated according to the geometric area of the GCE ($0.1256\ cm^2$).

2.4. Cell performance tests

Cell performance tests were carried out with a in-house fabricated alkaline DEFC using an electric load system (BT2000, Arbin Instrument, Inc.). The alkaline DEFC was composed of a MEA, with an active area of 1.0 cm × 1.0 cm, sandwiched between two bipolar plates, which were fixed by two fixture plates. Both plates were made of stainless steel and a single serpentine flow-field, 1.0 mm wide, 0.5 mm deep, and 1.0 mm wide in channel ribs, was formed on each fixture plate. The MEA consisted of an anion-exchange membrane and two electrodes. The membrane (A201) was provided by Tokuyama Corporation, while the cathode electrode consisted of a non-platinum HYPERMEC™ catalyst provided by Acta. To form the anode electrode, an anode ink was prepared by mixing 20 wt.% Pd/C or Pd_2Ni_3/C with 5 wt.% PTFE emulsion as a binder in ethanol [22]. Each catalyst ink was well-dispersed by the ultrasonic process and brushed on a nickel foam (Hohsen Corp., Japan), which served as the backing layer of the anode electrode. The Pd loading in the anode was $1.0\ mg\ cm^{-2}$. Cell performance tests were conducted at 60 °C, and two types of aqueous solution with different ethanol and KOH concentrations were pumped to the anode at a rate of $1.0\ mL\ min^{-1}$, while dry pure oxygen at a flow rate of 100 standard cubic centimeters per minute (sccm) was fed to the cathode. All the data were collected after the cell performance became stable.

3. Results and discussion

3.1. XRD, TEM, EDS and XPS characterizations of the Pd/C and PdNi/C catalysts

Bulk structural information for the Pd/C and PdNi/C catalysts with different Pd/Ni atomic ratios was obtained by XRD and is shown in Fig. 1. It can be seen that there are five common peaks for all the samples. The first broad peak, located at the 2θ value of about 25°, is referred to the graphite (0 0 2) facet of the carbon powder support, and the other four peaks around the 2θ values of 40.05°, 47.05°, 67.95°, and 82.10° are assigned to the (1 1 1), (2 0 0), (2 2 0) and (3 1 1) facets of the face-centered cubic (fcc) crys-

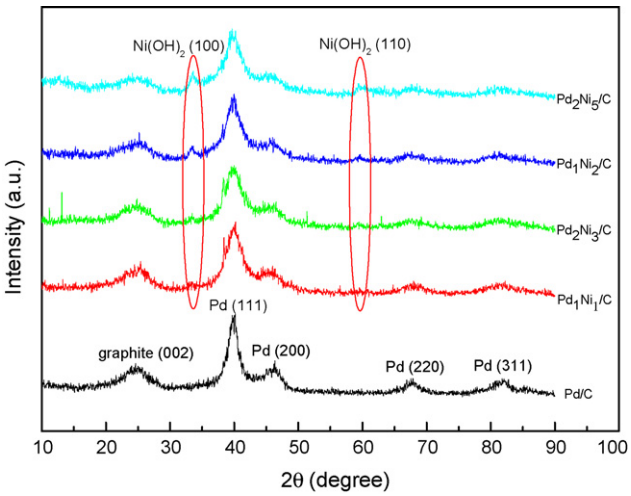

Fig. 1. XRD patterns of Pd/C and PdNi/C catalysts with different Pd:Ni atomic ratios.

talline Pd, respectively [23]. For the series of the PdNi/C catalysts, there also exist another two small peaks at 2θ values of about 33.5° and 59.2°, respectively, and their intensities increase with the Ni content, These peaks are attributed to $Ni(OH)_2$ (1 0 0) and (1 1 0) facets [24]. No significant shift is observed for all the PdNi/C catalysts, which suggests that Pd and Ni do not alloy well with this preparation method. It should be mentioned that during the synthesis of PtNi, PtRuNi and PtSnNi catalysts via a similar method [18–20], Ni was found to be well alloyed with Pt, thus lowering the Pt–CO binding energy. It is also noted from Fig. 1 that there are no diffraction peaks of metallic Ni, NiO or NiOOH for these PdNi/C catalysts, which indicates that Ni mostly exists in the form of $Ni(OH)_2$ using this preparation method; note that it was reported earlier that Ni mainly exists in the form of NiO in metal oxide promoted Pd catalysts prepared by IMH method [11]. The average size of the metal particles is calculated based on the broadening of the (2 2 0) diffraction peaks according to Scherrer's equation [25]:

$$d = \frac{0.9\lambda}{B_{2\theta} \cos \theta_{\max}} \quad (1)$$

where λ represents the wavelength of the X-ray, θ is the angle of the maximum peak, and $B_{2\theta}$ is the width of the peak at half height. The average size of Pd particles is 3.6 mm in Pd/C, 3.2 nm in Pd_1Ni_1/C, 3.1 nm in Pd_2Ni_3/C, 3.1 nm in Pd_1Ni_2/C, and 3.0 nm in Pd_2Ni_5/C.

Fig. 2a and b shows typical TEM images for the Pd/C and Pd_2Ni_3/C samples, respectively. The metal particles on both catalysts exhibit a spherical-like shape and are well-dispersed on the carbon powder support. Fig. 2c and d presents histograms of size distribution of the metal particles in Pd/C and Pd_2Ni_3/C catalysts, which were evaluated from an ensemble of 200 particles in an arbitrarily chosen area of the corresponding TEM images. According to the evaluation, both the Pd/C and Pd_2Ni_3/C catalysts have the same metal particle-size distribution that ranges from 2 to 8 nm, while the average metal particle size of Pd/C and Pd_2Ni_3/C are 3.8 and 3.7 nm, respectively.

The overall composition of the Pd_2Ni_3/C catalyst and the local composition of an individual metal particle were analyzed by EDS and are shown in Fig. 3. The EDS analysis over the entire region of Fig. 2b shows that the Ni:Pd atomic ratio of the Pd_2Ni_3/C catalyst is 1.30, while the EDS analysis of a single metal particle, which

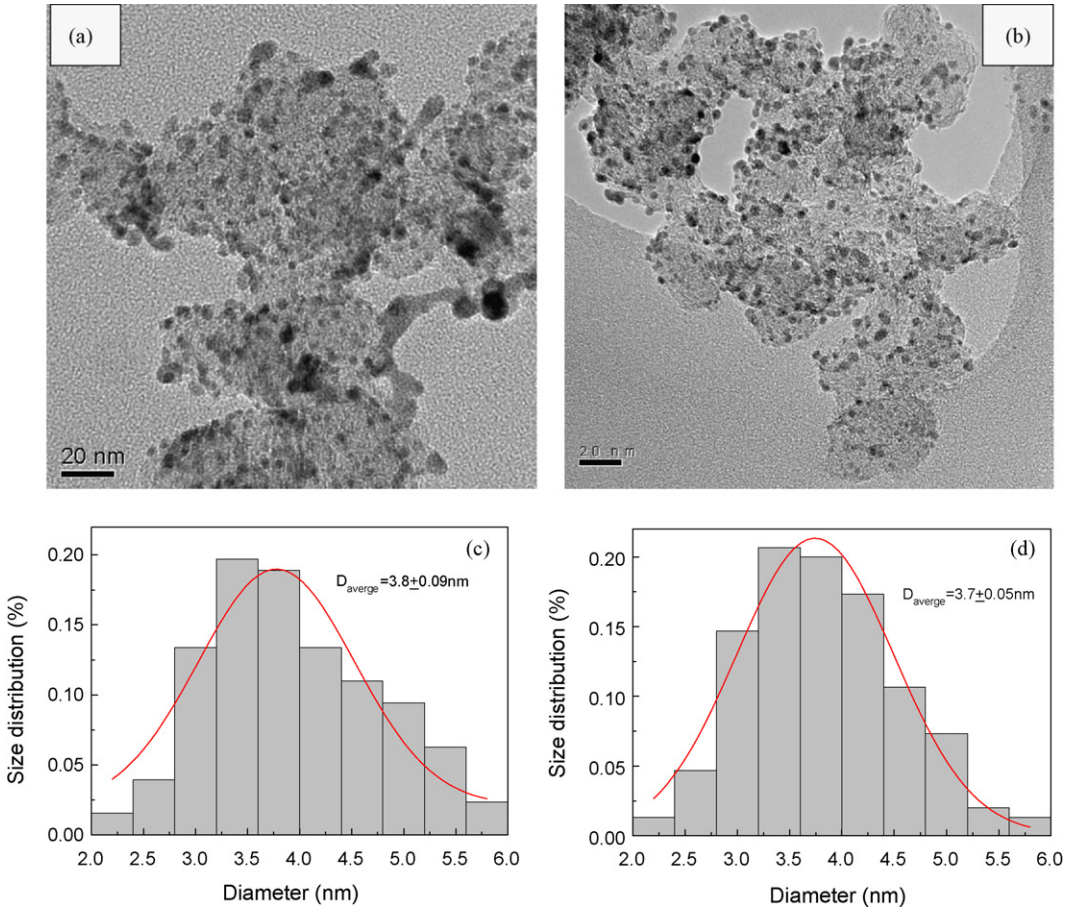

Fig. 2. TEM images (a and b) and histograms of metal particle-size distribution (c and d) for Pd/C and Pd_2Ni_3/C catalysts.

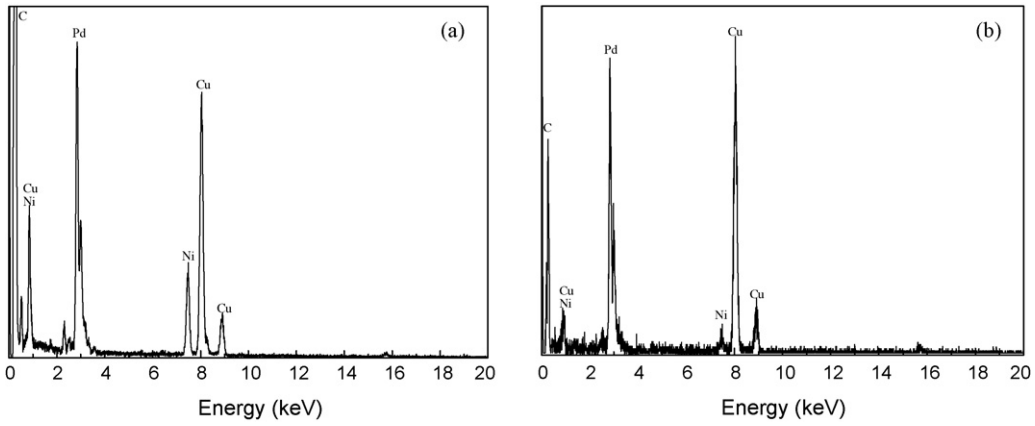

Fig. 3. EDS spectra of (a) Pd_2Ni_3/C catalyst and (b) an individual metal particle.

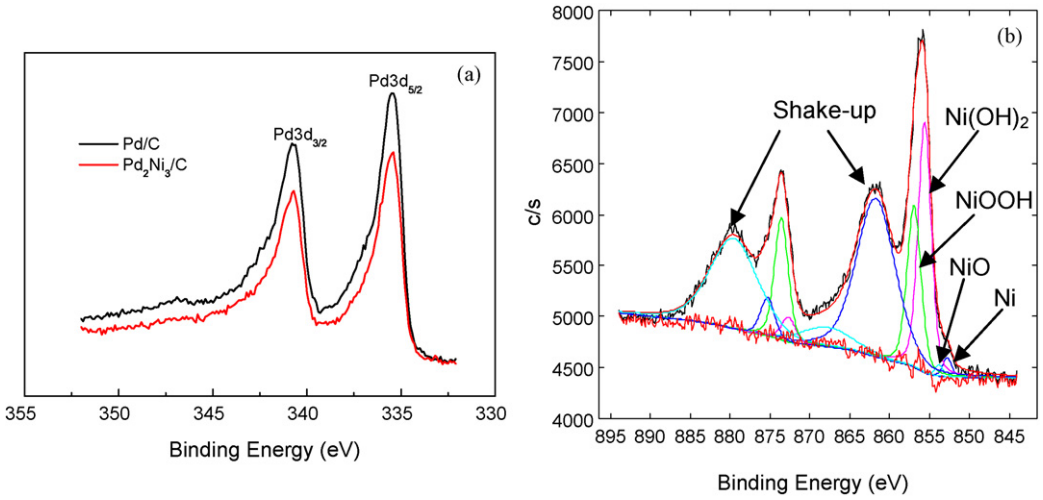

Fig. 4. XPS spectra of (a) Pd/C and Pd_2Ni_3/C and (b) Ni2p XPS spectrum of Pd_2Ni_3/C.

was chosen randomly from Fig. 2b, shows that the Ni:Pd atomic ratio is 1.34. The fact that Ni:Pd atomic ratio analyzed over a wide region is rather close to that analyzed for a randomly chosen single metal particle in the region suggests that the catalyst prepared using the simultaneous method ensures a homogeneous composition distribution. The ICP-AES analysis of the bulk composition of the Pd_2Ni_3/C catalyst reveals that the Ni:Pd atomic ratio is 1.28, which, like the result of the EDS analysis, is also slightly lower than the nominal ratio of 1.5 in the precursors.

XPS was employed to analyze the surface composition and the oxidation state of the metals in the Pd/C and Pd_2Ni_3/C catalysts. The regional spectra of the Pd 3d and Ni 2p core level regions are shown in Fig. 4. Surface composition analysis based on the intensities of XPS peaks of the Pd_2Ni_3/C catalyst shows that the Ni/Pd atomic ratio is 1.34, which is consistent with EDS analysis. In Fig. 4a, the Pd3d spectra display a doublet that consists of a high-energy band ($Pd3d_{3/2}$) and a low-energy band ($Pd3d_{5/2}$) at 340.8 and 335.5 eV for Pd/C, and 340.7 and 335.4 eV for Pd_2Ni_3/C. This observation indicates the existence of metallic state Pd. Unlike the case of PtNi, PtRuNi and PtSnNi reported elsewhere [18–20], the decrease in the Pd binding energy for Pd_2Ni_3/C relative to that of Pd/C is only 0.1 eV, i.e., negligibly small. This fact suggests that the change in the electronic structure of Pd is weak due to electron transfer from Ni to Pd, a conclusion that is consistent with the XRD analyses. As can be seen from Fig. 4b, the Ni2p spectrum of the Pd_2Ni_3/C catalyst shows a complicated structure by the presence of high binding energy satellite peaks adjacent to the main peaks, which can be attributed to multi-electron excitation [18]. Taking the shake-up peaks into account, the $Ni2p_{3/2}$ peak spectra are deconvoluted into four peaks at 852.7, 853.8, 855.6 and 857.3 eV, corresponding to metallic Ni, NiO, $Ni(OH)_2$ and NiOOH, respectively, and the corresponding XPS area ratios are 11.34, 4.81, 53.83, and 30.02%. The XPS area ratios of the chemical states of Ni species for all the PdNi/C catalysts are shown in Table 1. It can be seen that the Ni species are mainly comprised of $Ni(OH)_2$ and NiOOH for all the PdNi/C catalysts, and the ratios between them are similar.

Table 1
XPS area ratios of chemical states of Ni species for PdNi/C catalysts.

Samples	XPS area ratio (%)			
	Metallic Ni	NiO	$Ni(OH)_2$	NiOOH
Pd_1Ni_1/C	12.44	8.12	48.43	31.01
Pd_2Ni_3/C	11.34	4.81	53.83	30.02
Pd_1Ni_2/C	5.33	3.77	59.64	31.26
Pd_2Ni_5/C	2.55	3.40	64.43	29.62

3.2. Electrochemical measurements of Pd/C and PdNi/C catalysts

Fig. 5 compares typical CV curves of EOR on Pd/C and PdNi/C catalysts measured in 1.0 M KOH solution containing 1.0 M EtOH in the potential range from −0.926 to 0.274 V. The data show that

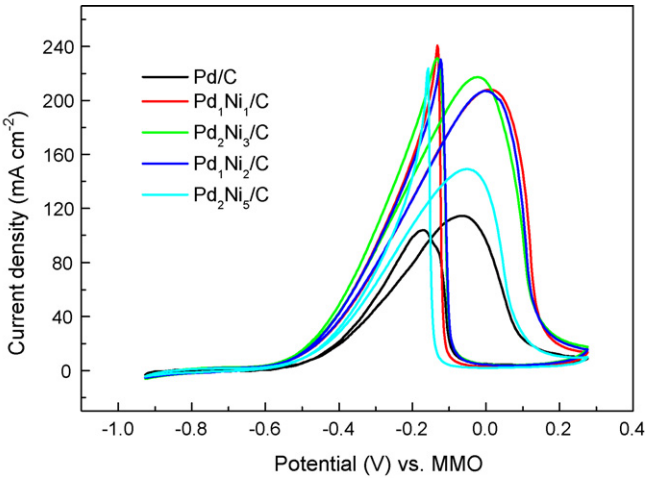

Fig. 5. CV curves of EOR on Pd/C and PdNi/C catalysts.

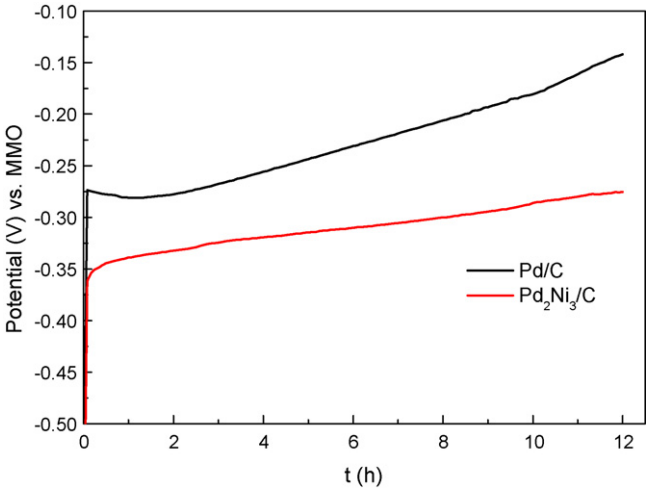

Fig. 6. Chronopotentiometric curves of EOR on Pd/C and Pd_2Ni_3/C catalysts at 20 mA cm^{-2}.

the addition of Ni at a certain content can significantly increase the catalytic activity of Pd. On the other hand, too great a content of Ni will cause the activity of the PdNi/C catalysts to decrease, primarily because the electronic conductivity of the catalyst decreases with Ni oxide/hydroxide. Among all the synthesized Pd/C and PdNi/C catalysts, the Pd_2Ni_3/C catalyst shows the highest activity toward EOR in alkaline media, compared with Pd/C and other PdNi catalysts, in terms of both the onset potential and the peak current density. The onset potential is −0.55 V for the Pd/C catalyst, and −0.65 V for the Pd_2Ni_3/C catalyst, while the peak current density for the Pd_2Ni_3/C catalyst is 217 mA cm^{-2}, which is about 103 mA cm^{-2} higher than that for the Pd/C catalyst. This indicates that the addition of Ni greatly enhances the kinetics of EOR on Pd in alkaline media. According to XRD and TEM analyses, the Pd/C and PdNi/C catalysts have the same metal particle-size distribution and the difference between their average metal particle sizes is rather small. Hence, the difference in the catalytic activity between the Pd/C and PdNi/C is independent of particle size. Both XRD and XPS show that little alloy occurs between Ni and Pd, which suggests that the electronic effect brought by the addition of Ni also contributes little to the high catalytic activity of the PdNi/C catalysts. Hence, the various oxidation states of Ni, which are uniformly distributed around Pd as attested by EDS, must account for the role of Ni as a catalytically enhancing agent toward EOR on Pd in alkaline media. It is generally believed that these Ni species are oxophilic like Ru, have the capacity to generate OH_{ads} at a lower potential, and facilitate the oxidative desorption of the intermediate products, thus enhancing both the catalytic activity and stability of Pd catalysts [26]. Previous studies [18–20] have revealed that the nickel hydroxides ($Ni(OH)_2$ and NiOOH) have a high electron and proton conductivity, and exhibit a high catalytic activity as heterogeneous catalysts. Other studies [27–29] have confirmed that the presence of Ni with different states has a beneficial effect on alcohol oxidation in either acidic or alkaline media. Here, the nickel hydroxides, the main component of the Ni species, may chiefly account for the great promotion of EOR on Pd in alkaline media through the reversible redox [30,31]:

$$Ni(OH)_2 + OH^- \Leftrightarrow NiOOH + H_2O + e^- \quad (2)$$

In addition, the nickel hydroxides can facilitate the oxidation of H_{ads} on a Pd surface via the hydrogen spillover effect [20]. The uniform distribution of the Ni species around Pd prepared by the simultaneous reduction method can also contribute to the catalytic activity compared with the two-step preparation method.

Fig. 6 shows the CP curves of the EOR on the Pd/C and Pd_2Ni_3/C catalysts, for which a constant current density of 20 mA cm^{-2} was applied for 12 h. As can be seen, the Pd_2Ni_3/C catalyst is more stable than Pd. The polarization potential gradually increases with time and through the same scanning time the Pd_2Ni_3/C catalyst shows a lower polarization potential than Pd/C. The curve for Pd_2Ni_3/C has a slope of 0.0069, which is only half that for Pd/C (0.0129). This observation indicates that the Pd_2Ni_3/C catalyst is more resistant to the poisoning caused by the intermediates. The higher capability in resisting poisoning of intermediates can be attributed to both the oxophilic Ni species and the transformation between $Ni(OH)_2$ and NiOOH.

3.3. Alkaline DEFCs cell performance test

The polarization and power density curves of alkaline DEFCs using Pd/C or Pd_2Ni_3/C as the anode catalyst are presented in Fig. 7. The measurements were made by feeding 1.0 M ethanol mixed with 1.0 M KOH to the fuel cell at 60 °C. The alkaline DEFC with a Pd_2Ni_3/C anode gives better performance than that with Pd/C in terms of both open-circuit voltage (OCV) and power density. In the case of Pd_2Ni_3/C, the OCV is 0.88 V, i.e., 0.18 V higher than that with Pd/C, which is consistent with the onset potential of EOR in CV characterization. The maximum power density for Pd_2Ni_3/C is 44 mW cm^{-2}, and that for Pd/C is 33 mW cm^{-2}. The polarization and power density curves of the alkaline DEFCs in a modest high concentration

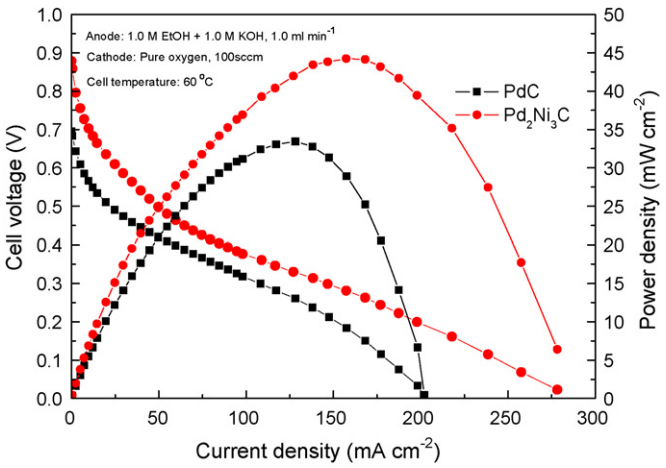

Fig. 7. Polarization and power density curves of alkaline DEFCs with different anode catalysts (anode: 1.0 M ethanol and 1.0 M KOH aqueous solution).

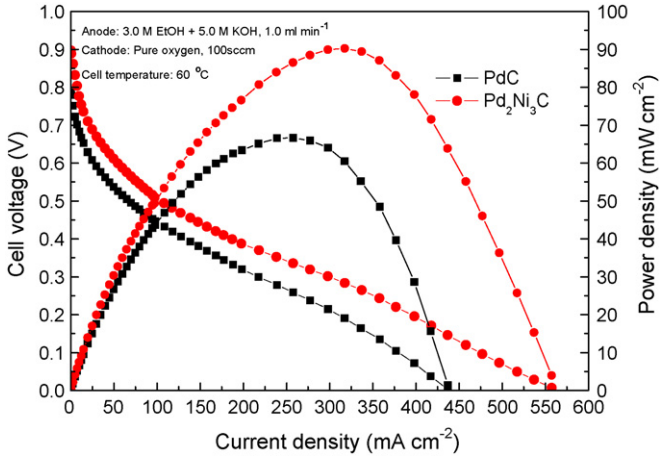

Fig. 8. Polarization and power density curves of alkaline DEFCs with different anode catalysts (anode: 3.0 M ethanol and 5.0 M KOH aqueous solution).

of solution (3.0 M ethanol mixed with 5.0 M KOH) [32] are given in Fig. 8. With the Pd_2Ni_3/C catalyst as an anode, the OCV is 0.89 V and the peak power density is 90 mW cm^{-2}, while in the case of Pd/C, the OCV is 0.79 V and the peak power density is 67 mW cm^{-2}. The results further confirm that the Pd_2Ni_3/C catalyst exhibits a higher catalytic activity toward EOR in alkaline media than the Pd/C catalyst.

4. Conclusions

PdNi/C catalysts have been successfully synthesized by the simultaneous reduction method using $NaBH_4$ as a reductant and have been characterized by different physicochemical methods. XRD analyses confirm the formation of face-centered cubic crystalline Pd and $Ni(OH)_2$ on the carbon powder for the PdNi/C catalysts. The TEM images show the well-dispersed metal particles on the carbon powder, and EDS data indicate a uniform distribution of composition. The CV and CP results demonstrate that the Pd_2Ni_3/C catalyst exhibits superior activity and stability toward EOR in alkaline media compared with the Pd/C catalyst, and the various oxidation states of Ni, which are uniformly distributed around Pd, account for the role of Ni as a catalytically enhancing agent toward EOR in alkaline media. Fuel cell performance tests demonstrate that the optimized Pd_2Ni_3/C catalyst prepared in this work is a promising anode catalyst for alkaline DEFCs by giving higher power density and high stability.

Acknowledgements

The work was fully supported by a grant from the Research Grants Council of the Hong Kong Special Administrative Region, China (Project No. 623008).

References

[1] E. Antolini, J. Power Sources 170 (2007) 1–12.
[2] S. Rousseau, C. Coutanceau, C. Lamy, J.-M. Léger, J. Power Sources 158 (2006) 18–24.
[3] F. Vigier, C. Coutanceau, F. Hahn, E.M. Belgsir, C. Lamy, J. Electroanal. Chem. 563 (2004) 81–89.
[4] J. Mann, N. Yao, A.B. Bocarsly, Langmuir 22 (2006) 10432–10436.
[5] Y. Paik, S.-S. Kim, O.H. Han, Electrochem. Commun. 11 (2008) 302–304.
[6] S.Q. Song, W.J. Zhou, Z.H. Zhou, L.H. Jiang, G.Q. Sun, Q. Xin, V. Leontidis, S. Kontou, P. Tsiakaras, Int. J. Hydrogen Energy 30 (2005) 995–1001.
[7] H.Q. Li, G.Q. Sun, L. Cao, L.H. Jiang, Q. Xin, Electrochim. Acta 52 (2007) 6622–6629.
[8] E.H. Yu, K. Scott, J. Power Sources 137 (2004) 248–256.
[9] T. Burchardt, P. Gouérec, E. Sanchez-Cortezon, Z. Karicchev, J.H. Miners, Fuel 81 (2002) 2151–2155.
[10] K. Matsuoka, Y. Iriyama, T. Abe, M. Matsuoka, Z. Ogumi, J. Power Sources 150 (2005) 27–31.
[11] P.K. Shen, C.W. Xu, Electrochem. Commun. 8 (2006) 184–188.
[12] C.W. Xu, Z.Q. Tian, P.K. Shen, S.P. Jiang, Electrochim. Acta 53 (2008) 2610–2618.
[13] V. Bambagioni, C. Bianchini, A. Marchionni, J. Filippi, F. Vizza, J. Teddy, P. Serp, M. Zhiani, J. Power Sources 190 (2009) 241–251.
[14] Z.X. Liang, T.S. Zhao, J.B. Xu, Electrochim. Acta 54 (2009) 2203–2208.
[15] C.W. Xu, P.K. Shen, Y.L. Liu, J. Power Sources 164 (2007) 527–531.
[16] F.P. Hu, C.L. Chen, Z.Y. Wang, G.Y. Wei, Electrochim. Acta 52 (2006) 1087–1091.
[17] J.Y. Xi, J.S. Wang, L.H. Yu, X.P. Qiu, L.Q. Chen, Chem. Commun. (2007) 1656–1658.
[18] K.-W. Park, J.-H. Choi, B.-K. Kwon, S.-A. Lee, Y.-E. Sung, H.-Y. Ha, S.-A. Hong, H.H. Kim, A. Wieckowski, J. Phys. Chem. B 106 (2002) 1869–1877.
[19] J.-H. Choi, K.-W. Park, B.-K. Kwon, Y.-E. Sung, J. Electrochem. Soc. 150 (2003) A973–A978.
[20] Z.B. Wang, P.J. Zuo, G.J. Wang, C.Y. Du, G.P. Yin, J. Phys. Chem. C 112 (2008) 6582–6587.
[21] E. Ribadeneira, B.A. Hoyos, J. Power Sources 180 (2008) 238–242.
[22] Y.S. Li, T.S. Zhao, Z.X. Liang, J. Power Sources 190 (2009) 223–229.
[23] S.D. Yang, X.G. Zhang, H.Y. Mi, X.G. Ye, J. Power Sources 175 (2008) 26–32.
[24] L. Xiao, J.T. Lu, P.F. Liu, L. Zhuang, J.E. Yan, Y.G. Hu, B.W. Mao, C.J. Lin, J. Phys. Chem. B 109 (2005) 3860–3867.
[25] J.B. Xu, T.S. Zhao, Z.X. Liang, J. Phys. Chem. C 112 (2008) 17362–17367.
[26] V. Bambagioni, C. Bianchini, J. Filippi, W. Oberhauser, A. Marchionni, F. Vizza, R. Psaro, L. Sordelli, M.L. Foresti, M. Innocenti, ChemSusChem. 2 (2009) 99–112.
[27] T.C. Deivaraj, W.X. Chen, J.Y. Lee, J. Mater. Chem. 13 (2003) 2555–2560.
[28] M.R. Tarasevich, Z.R. Karichev, V.A. Bogdanovskaya, E.N. Lubnin, A.V. Kapustin, Electrochem. Commun. 7 (2005) 141–146.
[29] J. Bagchi, S.K. Bhattacharya, J. Power Sources 163 (2007) 661–670.
[30] M.A. Abdel Rahim, R.M. Abdel Hameed, M.W. Khalil, J. Power Sources 134 (2004) 160–169.
[31] A.J. Motheo, S.A.S. Machado, F.J.B. Rabelo, J.R. Santos, J. Braz. Chem. Soc. 5 (1994) 161–165.
[32] Y.S. Li, T.S. Zhao, Z.X. Liang, J. Power Sources 187 (2009) 387–392.